When, how, and why the path of an air bubble rising in pure water becomes unstable

Paul Bonnefis, David Fabre, Jacques Magnaudet

When, how, and why the path of an air bubble rising in pure water becomes unstable

Paul Bonnefis[a], David Fabre[a], and Jacques Magnaudet[a,1]

Edited by Michael Manga, University of California, Berkeley, CA; received January 25, 2023; accepted February 7, 2023

Recently, [Herrada, M. A. and Eggers, J. G., Proc. Natl. Acad. Sci. U.S.A. 120, e2216830120 (2023)] reported predictions for the onset of the path instability of an air bubble rising in water and put forward a physical scenario to explain this intriguing phenomenon. In this Brief Report, we review a series of previously established results, some of which were overlooked or misinterpreted by the authors. We show that this set of findings provides an accurate prediction and a consistent explanation of the phenomenon that invalidates the suggested scenario. The instability mechanism actually at play results from the hydrodynamic fluid-body coupling made possible by the unconstrained motion of the bubble which behaves essentially, in the relevant size range, as a rigid, nearly spheroidal body on the surface of which water slips freely.

bubbles | hydrodynamic stability | numerical methods

Daily experience reveals that millimeter-sized air bubbles rising in still water generally follow zigzagging or spiraling paths rather than the expected rectilinear vertical trajectory. The physical processes governing this intriguing behavior have challenged fluid dynamicists since the early days of the discipline (1). Only recently has the combination of controlled laboratory experiments, direct numerical simulation, and global linear stability analysis led to the elucidation of this puzzle.

With water being a polar liquid, air–water interfaces are extremely sensitive to minute amounts of surfactants. This is why reference data for the onset of the path instability of air bubbles rising in ultrapure water have only been available for a few decades (2). These results reveal that, under standard conditions, the instability threshold is reached with bubbles of equivalent radius* $R \approx 0.91$ mm, which corresponds to a Bond number $Bo = \rho g (2R)^2/\gamma \approx 0.45$ and a Galilei number $Ga = \rho (2R)^{3/2} g^{1/2}/\mu \approx 243$, with $\rho = 10^3$ kg m^{-3}, $\mu = 10^{-3}$ kg.m^{-1}s^{-1}, and $\gamma = 7.28 \times 10^{-2}$ kg s^{-2} being the density, viscosity, and surface tension of water, respectively, and g denoting gravity. Predicting this threshold resisted repeated attempts until numerical codes capable of handling the global linear stability of the body+fluid system for bubbles that move and deform freely became available. Such a tool, based on an arbitrary Lagrangian–Eulerian formalism combined with a Newton method, was developed by Bonnefis (3); see ref. 4 for a technical overview. Results from ref. 3, obtained under the assumption that the flow past the bubble obeys a shear-free condition at the air–water interface, yield a critical radius $R_c = 0.927$ mm, implying $Bo_c = 0.463$ (Fig. 1*A*) and $Ga_c = 250$ (Figure 5.7 in ref. 3). This prediction, which differs from the experimental threshold of ref. 2 by only 2%, has just been confirmed by Herrada and Eggers (5) using a different numerical approach.

In ref. 3, path instability was shown to arise through a Hopf bifurcation, the frequency associated with the unstable nonaxisymmetric mode being $f = 6.28$ Hz at the threshold (Fig. 1*B*). The conclusions of ref. 5 are identical. The resulting bubble path may be a circular or flattened helix or a planar zigzag, depending on initial conditions and weakly nonlinear effects (6).

Increasing R, a second oscillatory mode with a much higher frequency becomes unstable at $Bo = 0.525$ (Fig. 1). This mode is axisymmetric and is associated with shape oscillations combining components with two and three wavelengths along the bubble perimeter in each vertical diametrical plane (Figure 5.19 in ref. 3). For $R = 1.08$ mm ($Bo = 0.63$), the previous low-frequency mode splits into two branches, both of which are stationary, i.e., nonoscillatory (Fig. 1).

Prior to ref. 3, several global stability analyses of the bubble motion and the surrounding flow were carried out by constraining the bubble to keep a frozen shape throughout its ascent (7, 8). In ref. 7, a strictly oblate spheroidal shape was prescribed,

*Radius of the sphere having the same volume $\mathcal{V}$ as the bubble, i.e., $R = (\frac{3}{4\pi}\mathcal{V})^{1/3}$.

Author affiliations: [a]Institut de Mécanique des Fluides de Toulouse, Université de Toulouse, CNRS, Toulouse 31400, France

Author contributions: D.F. and J.M. designed research; P.B. performed research; P.B., D.F., and J.M. analyzed data; and J.M. wrote the paper.

The authors declare no competing interest.

[1]To whom correspondence may be addressed. Email: jmagnaud@imft.fr.

Published March 10, 2023.

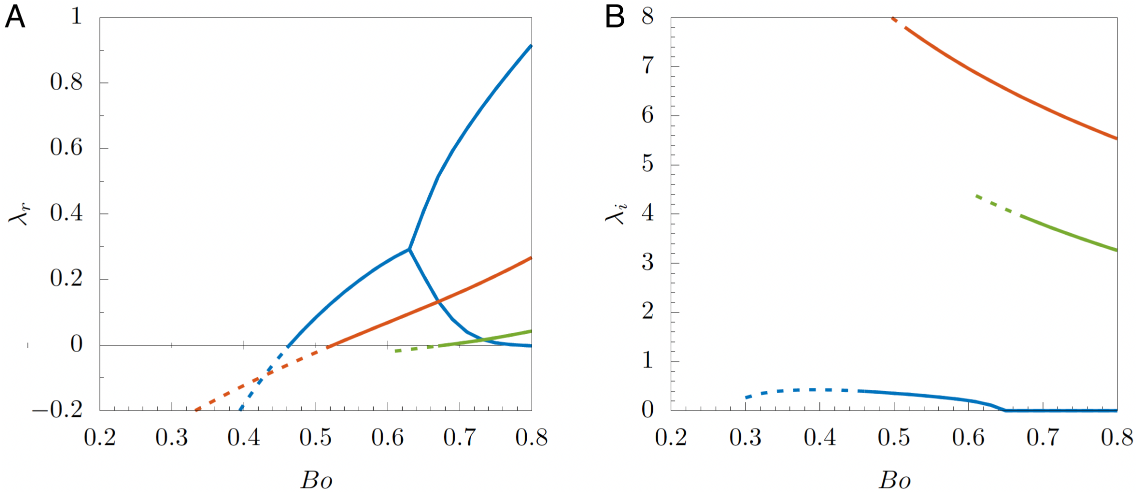

Fig. 1. Unstable eigenvalues of the system up to $Bo = 0.8$. (*A*) growth rate λ_r, normalized by the gravitational time $t_g = (R/g)^{1/2}$; (*B*) reduced frequency $\lambda_i = 2\pi f t_g$ ($t_g = 9.7 \times 10^{-3}$ s at the threshold). Adapted from Figure 5.15 of ref. 3.

while in ref. 8, the shape was computed by solving the axisymmetric Navier–Stokes equations. Then, this more realistic fore-aft asymmetrical shape was introduced in the global stability solver, together with the corresponding rise speed. Both studies concluded that, in the low-*Bo* high-*Ga* range relevant to millimeter-sized bubbles in water, the path first becomes unstable through a Hopf bifurcation. Increasing the bubble size, the nature of the most unstable mode was found to switch from oscillatory to stationary beyond a second threshold. Thus, the qualitative conclusions of refs. 7 and 8 are identical to those of ref. 3. Only the threshold and the associated oscillation frequency differ, Figure 7 of ref. 8 indicating critical conditions $Bo_c \approx 0.557$, $Ga_c \approx 287$ in the case of water. Compared with the prediction of ref. 3, this represents a mere 10% overestimate of the critical radius. As for the frequency at threshold (Figure 8 of ref. 8), it translates into $\lambda_i \approx 0.275$ in Fig. 1*B*, which is within 3% of the frequency predicted in ref. 3 for the nonaxisymmetric unstable mode at the same *Bo*. Last, in ref. 3, the instantaneous displacement of each point of the air–water interface was decomposed into a translation of the bubble centroid, a rigid-body rotation, and a volume-preserving deformation, the magnitude of each contribution being determined with a least-squares fitting technique. Figure 5.22 of ref. 3 reveals that the time-dependent deformations are about 300 times smaller than the horizontal displacements of the bubble centroid at the threshold. These various findings establish that, although deformations accounted for in refs. 3 and 5 but not considered in refs. 7 and 8 have some influence on the threshold of the path instability, they are by no means its cause, ruling

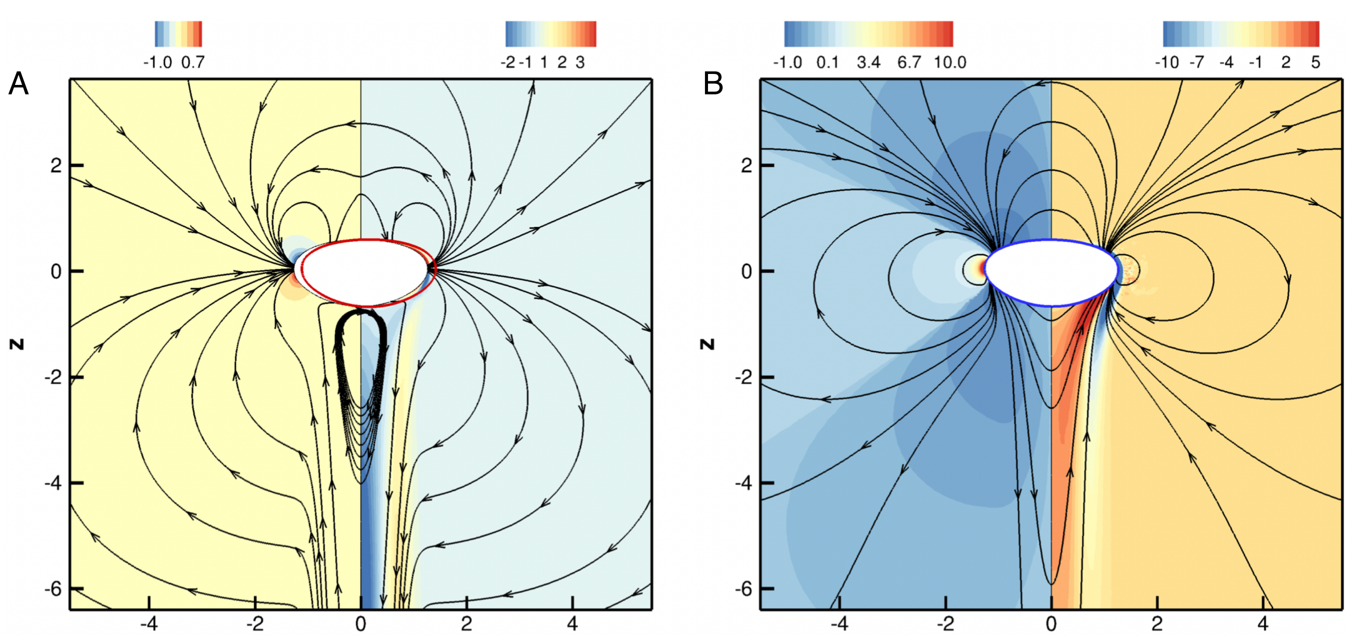

Fig. 2. Nonaxisymmetric unstable mode slightly above the threshold ($Bo = 0.48$). (*A*) real part, associated with the horizontal displacement of the bubble centroid; (*B*) imaginary part, associated with the rigid-body bubble rotation. Colors in the left and right halves of each frame correspond to isolevels of pressure and azimuthal vorticity disturbances, respectively. Streamlines are depicted with thin lines. The bubble aspect ratio is 1.98; the rotation-induced displacements of its surface are 14 times smaller than those due to its lateral translation. Reproduced from Figure 5.16 of ref. 3.

out the scenario developed in ref. 5 which is grounded on this causality.

To identify the actual origin of the instability, one has to compare the assumptions framework of refs. 7 and 8 with that of refs. 9 and 10 in which the stability of the wake of an oblate spheroidal bubble held fixed in a uniform stream was examined. In (9, 10), it was established that wake instability first arises through a stationary bifurcation when the bubble aspect ratio (ratio of the major and minor axes lengths) exceeds 2.21. Hence, in this constrained configuration, the nature of the primary bifurcation differs from that encountered with a freely rising bubble. Moreover, the critical bubble determined in ref. 3 has an aspect ratio slightly below 2.0 (Fig. 2), so that its wake is stable according to refs. 9 and 10.

That the bubble wake is still stable at the onset of path instability is typical of liquids characterized by a low value of the Morton number $Mo \equiv Bo^3/Ga^4 = g\mu^4/(\rho\gamma^3)$. Indeed, Figure 7 of ref. 8 reveals that bubbles with a realistic frozen shape rising in liquids such that $Mo \leq 1.2 \times 10^{-9}$ undergo path instability at a critical Galilei number somewhat lower than that at which their wake becomes unstable. The lower Mo, the larger the gap between the two critical Ga, so that this gap is significant for low-viscosity, high-surface-tension liquids such as water ($Mo = 2.54 \times 10^{-11}$).

From the above, it appears that neither wake instability nor time-dependent deformations are responsible for the path instability in the case of small bubbles rising in water. Consequently, the only explanation left is the coupling of the body and fluid motions which was not taken into account in refs. 9 and 10 but was in refs. 7 and 8 and turned out to change the nature of the primary bifurcation. Because of this coupling, flow disturbances influence the bubble motion through the surface distributions of pressure and viscous stress. Disturbances in the translational and angular bubble movements in turn influence the fluid motion through the boundary conditions at the bubble surface (Fig. 2). It is well-established for solid bodies, e.g., buoyancy-driven short cylinders and disks (11) or two-dimensional rods (12) that within certain parameter ranges, this fluid–body coupling makes the path of the body unstable via a Hopf bifurcation significantly below the wake instability threshold (see, e.g., Figure 15 in ref. 12). This is the essence of what happens to millimeter-sized bubbles rising in pure water.

Data, Materials, and Software Availability. Previously published data were used for this work, https://hal.science/tel-03982380v1/document, https://doi.org/10.1103/PhysRevFluids.7.113603, https://doi.org/10.1017/jfm.2014.340, http://dx.doi.org/10.1063/1.4939703, https://doi.org/10.1017/S0022112006003442 and https://doi.org/10.1017/jfm.2013.642.

1. J. Magnaudet, I. Eames, The motion of high-Reynolds-number bubbles in inhomogeneous flow. *Annu. Rev. Fluid Mech.* **32**, 659–708 (2000).
2. P. C. Duineveld, The rise velocity and shape of bubbles in pure water at high Reynolds number. *J. Fluid Mech.* **292**, 325–332 (1995).
3. P. Bonnefis, Ph.D. thesis, Institute National Polytechnic Toulouse, Toulouse, France (2019). https://hal.science/tel-03982380v1/document.
4. J. Sierra-Ausin, P. Bonnefis, A. Tirri, D. Fabre, J. Magnaudet, Dynamics of a gas bubble in a straining flow: Deformation, oscillations, self-propulsion. *Phys. Rev. Fluids* **7**, 113603 (2022).
5. M. A. Herrada, J. G. Eggers, Path instability of an air bubble rising in water. *Proc. Natl. Acad. Sci. U.S.A.* **120**, e2216830120 (2023).
6. J. Tchoufag, D. Fabre, J. Magnaudet, Weakly nonlinear model with exact coefficients for the fluttering and spiraling motion of buoyancy-driven bodies. *Phys. Rev. Lett.* **115**, 114501 (2015).
7. J. Tchoufag, J. Magnaudet, D. Fabre, Linear instability of the path of a freely rising spheroidal bubble. *J. Fluid Mech.* **751**, 1–12 (2014).
8. J. C. Cano-Lozano, J. Tchoufag, J. Magnaudet, C. Martinez-Bazán, A global stability approach to wake and path instabilities of nearly oblate spheroidal rising bubbles. *Phys. Fluids* **28**, 014102 (2016).
9. J. Magnaudet, G. Mougin, Wake instability of a fixed spheroidal bubble. *J. Fluid Mech.* **572**, 311–337 (2007).
10. J. Tchoufag, J. Magnaudet, D. Fabre, Linear stability and sensitivity of the flow past a fixed oblate spheroidal bubble. *Phys. Fluids* **25**, 054108 (2013).
11. J. Tchoufag, D. Fabre, J. Magnaudet, Global linear stability analysis of the wake and path of buoyancy-driven disks and thin cylinders. *J. Fluid Mech.* **740**, 278–311 (2014).
12. P. Assemat, D. Fabre, J. Magnaudet, The onset of unsteadiness of two-dimensional bodies falling or rising freely in a viscous fluid: a linear study. *J. Fluid Mech.* **690**, 173–202 (2011).